

This item is the archived peer-reviewed author-version of:

Optical spectrum of n-type and p-type monolayer MoS₂ in the presence of proximity-induced interactions

Reference:

Liu J., Xu W., Xiao Y.M., Ding L., Li H.W., Peeters François.- Optical spectrum of n-type and p-type monolayer MoS₂ in the presence of proximity-induced interactions

Journal of applied physics / American Institute of Physics - ISSN 1089-7550 - 134:22(2023), 224301

Full text (Publisher's DOI): <https://doi.org/10.1063/5.0181003>

To cite this reference: <https://hdl.handle.net/10067/2027770151162165141>

Optical spectrum of n -type and p -type monolayer MoS₂ in the presence of proximity-induced interactions

J. Liu,¹ W. Xu,^{2,1,3, a)} Y. M. Xiao,^{1, b)} L. Ding,¹ H. W. Li,² and F. M. Peeters^{2,4}

¹⁾*School of Physics and Astronomy and Yunnan Key laboratory of Quantum Information, Yunnan University, Kunming 650091, China*

²⁾*Micro Optical Instruments Inc., Shenzhen 518118, China*

³⁾*Key Laboratory of Materials Physics, Institute of Solid State Physics, HFIPS, Chinese Academy of Sciences, HFIPS, Hefei 230031, China*

⁴⁾*Department of Physics, University of Antwerp, Groenenborgerlaan 171, B-2020 Antwerpen, Belgium*

(Dated: 12 December 2023)

In this paper, we examined the effects of proximity-induced interactions such as Rashba spin-orbit coupling (SOC) and effective Zeeman fields (EZFs) on the optical spectrum of n -type and p -type monolayer (ML)-MoS₂. The optical conductivity is evaluated using the standard Kubo formula under Random phase approximation (RPA) with including the effective electron-electron interaction. It has been found that there exists two absorption peaks in n -type ML-MoS₂ and two knife shaped absorptions in p -type ML-MoS₂ which are contributed by the inter-subband spin flip electronic transitions within conduction and valence bands at valleys K and K' with a lifted valley degeneracy. The optical absorptions in n -type and p -type ML-MoS₂ occur in THz and infrared radiation regimes and the position, height, and shape of them can be effectively tuned by Rashba parameter, EZFs parameters, and carrier density. The interesting theoretical predictions in this study would be helpful for the experimental observation of the optical absorption in infrared to THz bandwidths contributed by inter-subband spin flip electronic transitions in a lifted valley degeneracy monolayer transition metal dichalcogenides (ML-TMDs) system. The obtained results indicate that ML-MoS₂ with the platform of proximity interactions make it a promising infrared and THz material for optics and optoelectronics.

I. INTRODUCTION

In recent years, the discovery of atomically thin two-dimensional (2D) materials such as graphene and monolayer transition metal dichalcogenides (ML-TMDs) has been an important and promising field of research in condensed matter physics¹⁻³. Due to the unique electronic and optical properties for potential applications in next generation of high-performance nanoelectronic devices and unique valleytronic features for information technology⁴⁻⁶, ML-TMDs have attracted much attention for scientific researches. The electronic structure of free-standing ML-TMDs is degenerated in K and K' valleys but with the opposite spin orientations⁷. The valley degeneracy of ML-TMDs can also be lifted via the exchange interaction induced by the proximity interaction in the presence of a ferromagnetic substrate⁸⁻¹¹. The proximity-induced 2D ML-TMD based valleytronic system has also led to the proposal to observe novel optical phenomena such as optical Hall effect and valley Hall effect^{11,12}.

The optical and transport properties of ML-MoS₂ have been theoretically and experimentally investigated^{2,4,11,13-18}. Previous theoretical results have indicated that the splittings of the conduction and valence bands of ML-MoS₂ in the presence of Rashba spin-orbit coupling (SOC) can introduce optical absorptions

in terahertz (THz) to infrared bandwidths¹⁵. The breaking of inversion symmetry at the surface or interface with the resultant electric field couples to the spin of itinerant electrons is called the Rashba effect¹⁹. The Rashba effect can lead to momentum-dependent splitting of spin bands and would enable spin-flip electronic transitions^{20,21}. It has been shown that the optical properties such as collective excitations and optical conductivity of traditional 2D system can be greatly influenced by the Rashba effect²²⁻²⁶. Moreover, the proximity-induced exchange interaction that introduced the effective Zeeman fields (EZFs) can lift the electronic energy spectrum by breaking the valley degeneracy^{8,11}. In order to understand the effect of proximity-induced exchange interaction on the optoelectronic property of ML-TMDs, it is necessary to examine the roles played by the Rashba SOC and EZFs.

In this study, we evaluate the dependence of longitudinal optical conductivity on the proximity-induced interactions under the linear polarized radiation field. The absorption spectrum (optical conductivity) is calculated via the Kubo formalism under the standard random-phase approximation (RPA) by including the effective electron-electron interaction. With considering the contributions of inter-subband spin-flip electronic transitions within conduction and valence bands in different valleys, the effects of n - and p -types doping (for varying carrier density via chemical doping or applying a gate voltage), EZFs, and the Rashba SOC strength on the optical conductivity of ML-MoS₂ at low temperature are investigated.

The paper is organized as follows. In Sec. II, the eigenvalues and wavefunctions of ML-MoS₂ in the pres-

^{a)}Electronic mail: wenzu_issp@aliyun.com

^{b)}Electronic mail: yiming.xiao@ynu.edu.cn

ence of proximity-induced interactions such as EZFs and the Rashba SOC are obtained by solving the Schrödinger equation. The optical conductivity of ML-MoS₂ is calculated through the Kubo formulism with the dynamical dielectric function under RPA. The numerical results of optical conductivity for different doping types, carrier density, the strengths of EZFs and Rashba SOC are presented and discussed in Sec. III. The concluding remarks are summarized in Sec. IV.

II. THEORETICAL FRAMEWORK

In this study, we consider ML-MoS₂ placed on a ferromagnetic substrate such as EuO or EuS where the proximity-induced interactions can lead to an enhanced valley splitting and spin-orbit coupling (SOC)¹¹. The low-energy effective Hamiltonian is written in the form of a 4×4 matrix as

$$H(\mathbf{k}) = \frac{1}{2} \times \begin{bmatrix} \Delta + d_\zeta^c & 2Ak_\zeta^- & 0 & i(1-\zeta)\lambda_R \\ 2Ak_\zeta^+ & -(\Delta - d_\zeta^v) & -i(1+\zeta)\lambda_R & 0 \\ 0 & i(1+\zeta)\lambda_R & \Delta - d_\zeta^c & 2Ak_\zeta^- \\ -i(1-\zeta)\lambda_R & 0 & 2Ak_\zeta^+ & -(\Delta + d_\zeta^v) \end{bmatrix}, \quad (1)$$

where $\mathbf{k} = (k_x, k_y)$ is the electron wavevector along the 2D-plane, $k_\zeta^\pm = \zeta k_x \pm ik_y$, $d_\zeta^\beta = \zeta \lambda_\beta - B_\beta$, and $\beta = (c, v)$. Here, $\zeta = \pm$ refers to the K (K') valley, $A = at$ with a being the lattice parameter and t the hopping parameter⁴. The intrinsic SOC parameters $2\lambda_c$ and $2\lambda_v$ are the spin splitting, respectively, at the bottom of the conduction band and at the top of the valence band in the absence of the Rashba SOC^{12,27-30}, B_c and B_v are effective Zeeman fields experienced by electrons in the conduction band and holes in valence band in the presence of exchange interaction induced by the substrate. Δ is the direct bandgap between the valence and conduction bands^{12,13,31}, and $\lambda_R = \alpha_R \Delta / (2at)$ with α_R being the Rashba coefficient^{32,33}. After solving the Schrödinger equation, one can obtain the eigenvalues and eigenfunctions of electrons or holes in ML-MoS₂.

The four eigenvalues $E_{\beta,s}^\zeta(\mathbf{k})$ are the solutions of the diagonalized equation

$$E^4 - A_2 E^2 + A_1 E + A_0 = 0, \quad (2)$$

with

$$\begin{aligned} A_2 &= \frac{\Delta^2}{2} + \lambda_R^2 + 2A^2 k^2 + \frac{d_\zeta^{v2} + d_\zeta^{c2}}{4}, \\ A_1 &= \frac{\Delta}{4} (d_\zeta^{v2} - d_\zeta^{c2}) - \frac{\zeta \lambda_R^2}{2} (d_\zeta^v - d_\zeta^c), \\ A_0 &= \left(\frac{\Delta^2}{4} + A^2 k^2 \right)^2 + \frac{\lambda_R^2}{4} (\Delta + \zeta d_\zeta^c) (\Delta + \zeta d_\zeta^d) \\ &\quad - \frac{\Delta^2}{16} (d_\zeta^{c2} + d_\zeta^{v2}) - \frac{A^2 k^2}{2} d_\zeta^c d_\zeta^v + \frac{(d_\zeta^c d_\zeta^v)^2}{16}, \end{aligned}$$

and the corresponding eigenfunctions for electronic states near the K and K' points are

$$|\mathbf{k}; \lambda \rangle = \mathcal{A}_{\beta,s}^\zeta [c_1, c_2, c_3, c_4] e^{i\mathbf{k} \cdot \mathbf{r}}, \quad (3)$$

where $\mathbf{r} = (x, y)$, $\lambda = (\beta, \zeta, s)$,

$$\begin{aligned} c_1 &= i\lambda_R [h_1 + 4A^2(1+\zeta)(k_\zeta^-)^2], \\ c_2 &= -4iA\lambda_R k_\zeta^- h_2, \\ c_3 &= 2Ak_\zeta^- h_3, \\ c_4 &= -[(\Delta - 2E)^2 - (d_\zeta^c)^2](\Delta + 2E - d_\zeta^v) \\ &\quad - (1+\zeta)^2 \lambda_R^2 (\Delta - 2E + d_\zeta^c) \\ &\quad - 4A^2 k^2 (\Delta - 2E - d_\zeta^c), \end{aligned}$$

and

$$\mathcal{A}_{\beta,s}^\zeta(\mathbf{k}) = (|c_1|^2 + |c_2|^2 + |c_3|^2 + |c_4|^2)^{-1/2},$$

is the normalization factor. Here, $h_1 = (1-\zeta)[\Delta - 2E_{\beta,s}^\zeta(\mathbf{k}) - d_\zeta^c][\Delta + 2E_{\beta,s}^\zeta(\mathbf{k}) - d_\zeta^v]$, $h_2 = \Delta - 2E_{\beta,s}^\zeta(\mathbf{k}) + \zeta d_\zeta^c$, and $h_3 = [\Delta - 2E_{\beta,s}^\zeta(\mathbf{k}) + d_\zeta^c][\Delta + 2E_{\beta,s}^\zeta(\mathbf{k}) - d_\zeta^v] + 4A^2 k^2$.

Therefore, we consider the carriers in ML-MoS₂ as spin-splitting 2D electron gas (2DEG) in the conduction band or 2D hole gas (2DHG) in the valence band with a two band mode. Here, we use a simplified form $E_s^\zeta(\mathbf{k}) = E_{\beta,s}^\zeta(\mathbf{k})$ and $\mathcal{A}_s^\zeta(\mathbf{k}) = \mathcal{A}_{\beta,s}^\zeta(\mathbf{k})$ for both conduction and valence subbands. With the energy spectrum of a spin-split 2DEG or 2DHG, the electron density-density ($d-d$) correlation function can be obtained, in the absence of $e-e$ screening, as^{29,34}

$$\Pi_\alpha^\zeta(\Omega, \mathbf{q}) = \sum_{\mathbf{k}} \frac{A_\alpha^\zeta(\mathbf{k}, \mathbf{q}) [f(E_{s'}^\zeta(\mathbf{k} + \mathbf{q})) - f(E_s^\zeta(\mathbf{k}))]}{E_{s'}^\zeta(\mathbf{k} + \mathbf{q}) - E_s^\zeta(\mathbf{k}) + \hbar\Omega + i\delta}, \quad (4)$$

where

$$\begin{aligned} A_{s's'}^\zeta(\mathbf{k}, \mathbf{q}) &= [A_{s'}^\zeta(\mathbf{k} + \mathbf{q}) A_s^\zeta(\mathbf{k})]^2 \sum_{i=1}^4 c_{is}^{\zeta*}(\mathbf{k}) c_{is'}^\zeta(\mathbf{k} + \mathbf{q}) \\ &\quad \times \sum_{j=1}^4 c_{js'}^{\zeta*}(\mathbf{k} + \mathbf{q}) c_{js}^\zeta(\mathbf{k}), \end{aligned} \quad (5)$$

is the structure factor. Here, $\alpha = (s's)$ is defined for electronic transition channel from the s branch to the s' branch with $s=\pm 1$ referring to different spin branches. $\zeta=\pm 1$ is for different valley, $\hbar\Omega$ is the excitation photon energy, and $\mathbf{q}=(q_x, q_y)$ is the change of electron wavevector during an $e-e$ scattering event. $f(x) = [e^{(x-E_F)/k_B T} + 1]^{-1}$ is the Fermi-Dirac function with E_F being the Fermi energy at zero temperature or chemical potential at a finite temperature. The dynamical RPA dielectric function hereby writes

$$\epsilon(\Omega, q) = 1 + a_1 + a_2 + a_3 + a_4. \quad (6)$$

Here, $(s's)=1=(++)$, $2=(+-)$, $3=(-+)$, and $4=(--)$ are defined for different transition channels, $(s's)=1$ and

4 (2 and 3) are for intra-band (inter-subband) transitions, $a_{s's} = -V_q \Pi_{s's}^{\zeta}(\Omega, q)$, and $V_q = 2\pi e^2 / \kappa q$ with κ being the dielectric constant of the material.

The RPA dielectric function can be used to calculate the effective interaction for optical response with different scattering events. In the presence of e - e interaction, the effective d - d correlation function becomes

$$\tilde{\Pi}_{\alpha}^{\zeta}(\Omega, \mathbf{q}) = \Pi_{\alpha}^{\zeta}(\Omega, q) / \epsilon(\Omega, q). \quad (7)$$

Using the Kubo formula in the absence of electronic scattering centers (such as impurities and phonons), the optical spectrum or optical conductivity of a spin-valley-splitting 2DEG (2DHG) can be calculated through^{24,34}

$$\sigma(\Omega) = - \lim_{q \rightarrow 0} \frac{e^2 \Omega}{q^2} \sum_{\zeta, \alpha} \text{Im} \tilde{\Pi}_{\alpha}^{\zeta}(\Omega, q). \quad (8)$$

In the present study, $\sigma(\Omega)$ is induced by current-current correlation via electron-electron interaction with the external electromagnetic field, which normally does not change the wavevector for a carrier. In the long-wavelength limit ($q \rightarrow 0$) and low temperature ($T \rightarrow 0$ K), the intra-band electronic transitions would not contribute to the optical conductivity. Moreover, strong optical absorptions can occur via inter-subband spin-flip transitions, especially for transitions from an energy lower spin branch to an energy higher spin branch at K and K' valleys.

III. RESULTS AND DISCUSSIONS

In numerical calculations, we consider the case at low temperature ($T \rightarrow 0$ K) to calculate the optical conductivity and take the following parameters for ML-MoS₂ with $A = 3.5123$ ÅeV, $\Delta = 1.66$ eV, $\lambda_c = -1.5$ meV, and $\lambda_v = 75$ meV^{13,35}. Usually, the Rashba parameter λ_R depends on the type of the substrate and can also be tuned through, e.g., applying a gate voltage³⁶. A large Rashba parameter $\lambda_R = 72$ meV was found in ML-MoTe₂ placed on an EuO substrate⁸. The EZFs factors B_c and B_v also depend on the types of substrates³⁷. For n -type ML-MoS₂, we take the spin relaxation time for inter-subband spin-flip transitions as $\tau_e = 3$ and $\tau_h = 300$ ps for p -type ML-MoS₂³⁸. With the energy relation approximation, one can replace the δ function in Eq. (4) with a Lorentzian distribution: $\delta(E) \rightarrow (E_{\tau}/\pi)/(E^2 + E_{\tau}^2)$, where $E_{\tau} = \hbar/\tau$ is the width of the distribution³⁹. It should be noted that energy relaxation time is a frequency-dependent parameter and is usually set to a constant for numerical calculation⁴⁰. We take the dielectric constants for air, bare ML-MoS₂ sheet, and bare EuO substrate as $\kappa_{\text{air}} = 1$, $\kappa_{\text{TMD}} = 3.3$ ⁴¹, and $\kappa_{\text{EuO}} = 23.9$ ⁴², respectively. The chemical potential $\mu_{e/h}$ for electrons in n -type and holes in p -type ML-MoS₂ can be determined through

$$n_e = \sum_{\zeta=\pm 1, s=\pm 1} \sum_{\mathbf{k}} f(E_s^{\zeta}(\mathbf{k})), \quad (9)$$

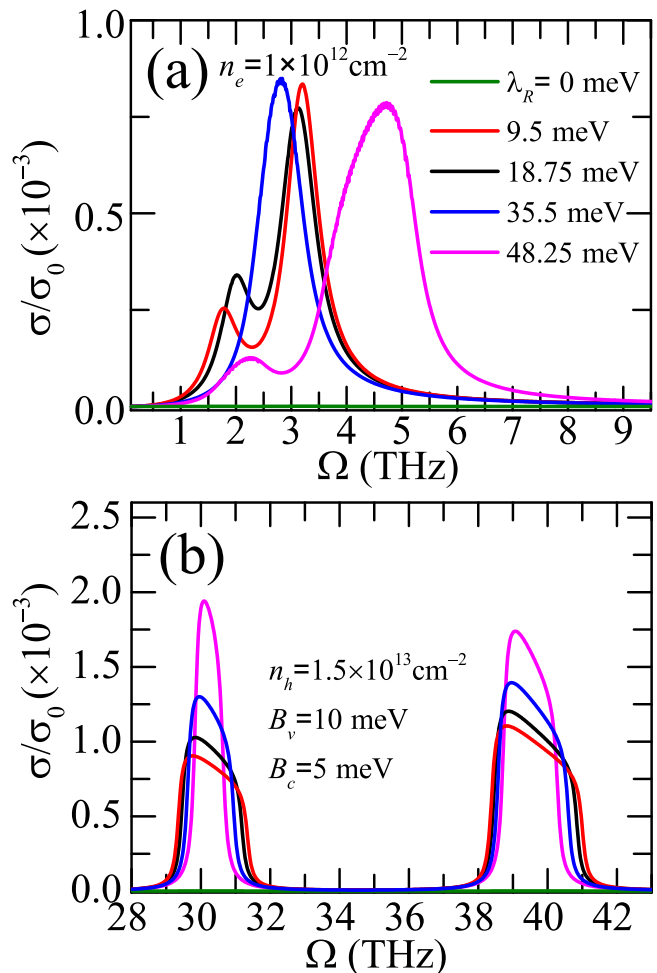


FIG. 1. Optical conductivity $\sigma(\Omega)$ as a function of radiation frequency Ω at a fixed carrier density (a) $n_e = 10^{12}$ cm⁻² for n -type and (b) $n_h = 1.5 \times 10^{13}$ cm⁻² for p -type ML-MoS₂ with $B_v = 10$ and $B_c = 5$ meV for different Rashba parameters λ_R as indicated. Here, $\sigma_0 = e^2/(4\hbar)$ is the universal optical conductivity of graphene.

and

$$n_h = \sum_{\zeta=\pm 1, s=\pm 1} \sum_{\mathbf{k}} [1 - f(E_s^{\zeta}(\mathbf{k}))], \quad (10)$$

respectively. As we know, the longitudinal optical conductivity of ML-MoS₂ on a ferromagnetic substrate in the presence of proximity-induced interactions can be measured by the infrared spectroscopy and THz TDS measurement. The theoretical model in this study provides an excellent platform to examine the optical absorption property by tuning the parameter such as Rashba parameter λ_R , EZFs B_c and B_v , and carrier density.

In Fig. 1, we plot the optical conductivity of n -type and p -type ML-MoS₂ as a function of radiation frequency Ω at fixed carrier density $n_e = 10^{12}$ cm⁻² for electrons and $n_h = 1.5 \times 10^{13}$ cm⁻² for holes, $B_c = 5$ meV, and $B_v = 10$ meV for different Rashba parameters λ_R . In Fig. 1(a), we find that there exist two absorption peaks

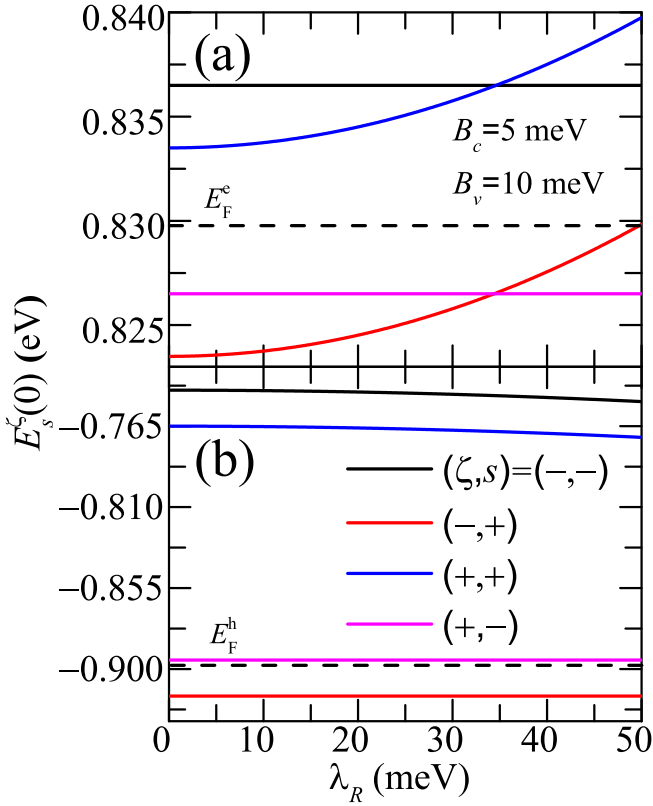


FIG. 2. (a) The minimum of the four conduction subbands ($\zeta = \pm, s = \pm$) and (b) the maximum of the four valence subbands as a function of Rashba parameter λ_R for fixed EZFs $B_v = 10$ and $B_c = 5$ meV at $k = 0$.

where the lower left peak is induced by spin-flip electronic transitions within K valley and the higher right peak is attributed to spin-flip electronic transitions within K' valley. With increasing λ_R , for $\lambda_R < 35.5$ meV, the lower left absorption peak blueshifts to higher frequencies and the higher right peak redshifts to lower frequencies. For $\lambda_R = 35.5$ meV, there is only one absorption peak because the band structure is valley degenerated in this case. While for $\lambda_R > 35.5$ meV, the higher peak redshifts to lower frequencies and the lower peak blueshifts to higher frequencies with increasing λ_R . In Fig. 1(b), there are two roughly knife shaped spectral absorptions in the infrared regime. With increasing λ_R , the widths of the knife shaped absorptions decrease and the heights of the knife shaped absorptions increase. In the absence of Rashba effect ($\lambda_R = 0$ meV), we notice that the optical conductivity approaches to zero because the spin-flip transitions are prohibited in this case.

The interesting findings in Fig. 1(a) can be understood with the help of Fig. 2(a) where we show the lowest energies at the bottom of four conduction subbands ($\zeta = \pm, s = \pm$) as a function of Rashba parameter λ_R for fixed EZFs $B_c = 5$ meV and $B_v = 10$ meV. With increasing λ_R , the energy spacing $E_+^+(0) - E_-^+(0)$ in valley K becomes larger and the energy spacing $E_-^-(0) - E_+^-(0)$ in

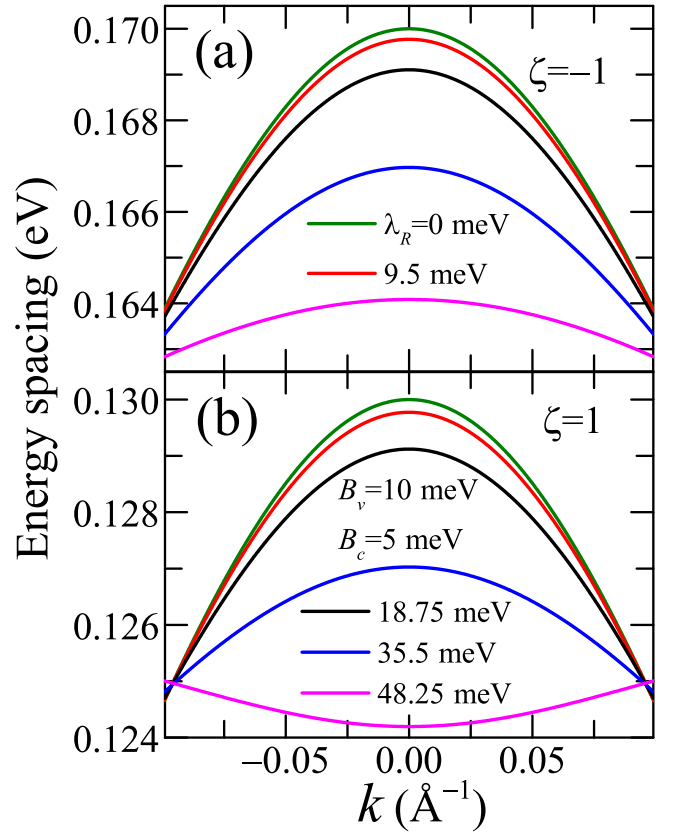


FIG. 3. The energy spacing between two spin splitting valence subbands as a function of wavevector k in (a) K' valley and (b) K valley with different Rashba parameters λ_R .

valley K' decreases, which would result in the blueshifts and redshifts of the two absorption peaks. In Fig. 2(b), we show the highest energies at the top of four valence subbands ($\zeta = \pm, s = \pm$) as a function of Rashba parameter λ_R for fixed EZFs $B_c = 5$ meV and $B_v = 10$ meV. As we can see, the Rashba parameter affects slightly the top points of them. At a fixed carrier density, we can see that the Fermi level for electrons/holes depends weakly on Rashba parameter, which are in line with the situation we had discussed previously¹⁵. Thus, the modification of the band structure by the Rashba effect would change the energy spacing between spin splitting subbands near the Fermi level and would result in the tuning of absorption peaks or knife shapes in Fig. 1. In Fig. 3, we also plot the energy spacing between two spin splitting subbands in the valence band for K and K' valleys to clearly clarify the Rashba effect on p -type sample. The Rashba effect would affect the energy spacing between the spin splitting valence subbands. With increasing λ_R , the region of energy spacing near the Fermi level becomes narrower. Thus, the knife shaped spectral absorptions in Fig. 1(b) also get narrower with increasing λ_R . The right boundaries of the two knife shape absorptions correspond to the highest energies in Figs. 3(a)-(b) for the largest electronic transition energies re-

quired by optical absorptions in p -type sample. As we can see, the regions and values of energy spacings in Fig. 3(a) are larger and higher than those in Fig. 3(b). As a consequence, the left and right knife shaped absorptions in Fig. 1(b) are contributed by the spin-flip electronic transitions in valleys K and K' , respectively, and the right knife shaped absorption is more wider than the left one. The strengths of the knife shaped absorptions also increase with increasing λ_R . It should be noted that the electronic band structure in ML-MoS₂ modified by EZFs and Rashba SOC have some differences from traditional 2DEG or 2DHG system in the presence of Rashba effect. Thus, the optical spectrum has both commons and differences with traditional 2DEG and 2DHG^{24,26}. In general, the Rashba effect can play an important and peculiar role in affecting and tuning the optical absorptions in THz and infrared bandwidths for n - and p -type ML-MoS₂ in the presence of proximity-induced exchange interaction.

The optical conductivity of n - and p -type ML-MoS₂ is shown in Fig. 4 as a function of radiation frequency Ω at fixed carrier density and λ_R for different EZFs. In Fig. 4(a), with a fixed $B_c = 10$ meV, we find that the width of absorption regime in optical conductivity curve increases and both of the two absorption peaks blueshift with increasing B_c . The strengths of two absorption peaks also become stronger with increasing B_c . For $B_c = 0$ meV, there exists only one peak because the conduction bands in K and K' valleys are degenerated in this case. For the optical spectrum for p -type ML-MoS₂ shown in Fig. 4(b), there is only one knife shape absorption when $B_v = 0$ meV because of the valley degeneracy of valence bands in K and K' valleys. For $B_v > 0$ meV, there are two knife shape absorptions. With increasing B_v , the left knife shape absorption redshifts and the width of it becomes more narrower. Meanwhile, the right one blueshifts and the width of it becomes more broader.

In Fig. 5, we plot the optical conductivity of n -type and p -type ML-MoS₂ as a function of radiation frequency Ω for fixed $\lambda_R = 18.75$ meV, EZFs $B_c = 5$ meV and $B_v = 10$ meV for different carrier densities. For ML-MoS₂, n -type and p -type doping samples can be realized through the field effect with different source and drain contacts^{17,43} and the doping levels can be tuned through, e.g., applying a gate voltage. Usually, one can reach high carrier density in experiment^{43,44} and we choose the carrier density with a magnitude of 10^{12} cm⁻² and hole density 10^{13} cm⁻² in our numerical calculation. In Fig. 5(a), we can see that both of the two absorption peaks have blueshifts to higher frequencies and the strengths of them become stronger with increasing electron density n_e . Two knife shaped absorptions in Fig. 5(b) become wider and their left boundaries move to the low frequency region with increasing hole density n_h . The left boundaries of two knife shape absorptions are redshifts with increasing carrier density because the chemical potential for holes in p -type sample decreases which allows the spin-flip transitions in the lower frequency regime. The

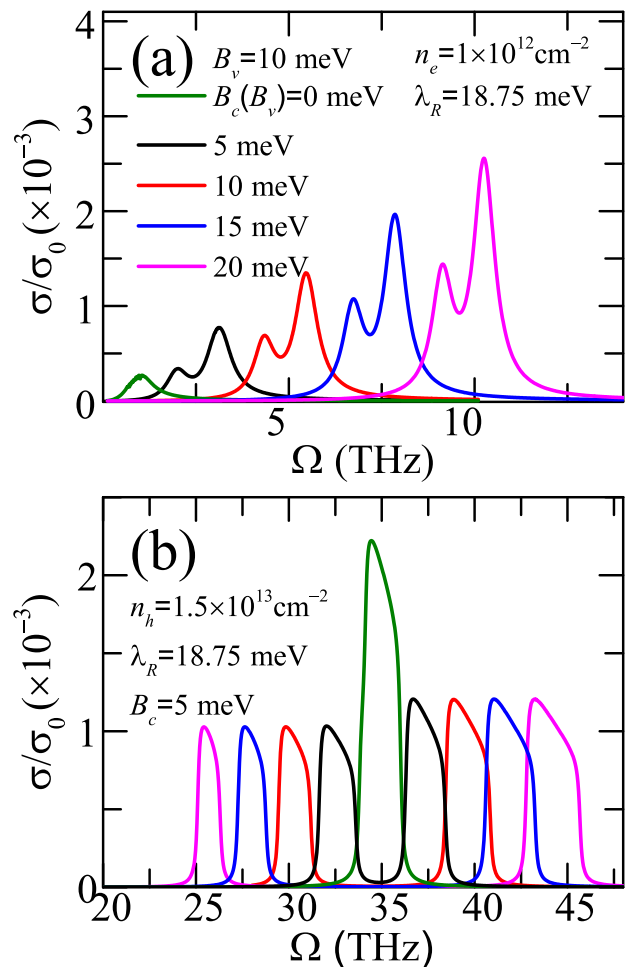


FIG. 4. (a) Optical conductivity $\sigma(\Omega)$ as a function of radiation frequency Ω at a fixed carrier density $n_e = 10^{12}$ cm⁻², EZFs parameter $B_v = 10$ meV, and Rashba parameter $\lambda_R = 18.75$ meV for n -type ML-MoS₂ with different EZF parameters B_c as indicated. (b) Optical conductivity $\sigma(\Omega)$ as a function of excitation frequency Ω at a fixed hole density $n_h = 1.5 \times 10^{13}$ cm⁻², EZFs parameter $B_c = 5$ meV, and Rashba parameter $\lambda_R = 18.75$ meV for p -type ML-MoS₂ with different EZF parameters B_v as indicated.

width of the right knife shaped absorption in Fig. 5(b) is wider than the left one because the region of energy spacing $E^-(k) - E^+(k)$ in valley K' is larger than $E^+(k) - E^-(k)$ in valley K . The interesting findings in Fig. 5 are due to the Pauli blockade effect with changing the carrier density⁴⁵. These theoretical results show that the optical absorption of ML-MoS₂ in THz and infrared regimes can also be effectively tuned by varying the carrier density.

It should be noted that in our present study, the optical spectrum is mainly determined by electronic transitions through e - e interaction at low temperature which is an ideal case where the electronic scattering mechanisms (e.g., impurities and phonons) are not taken into account. However, the shape and amplitude of optical conductivity

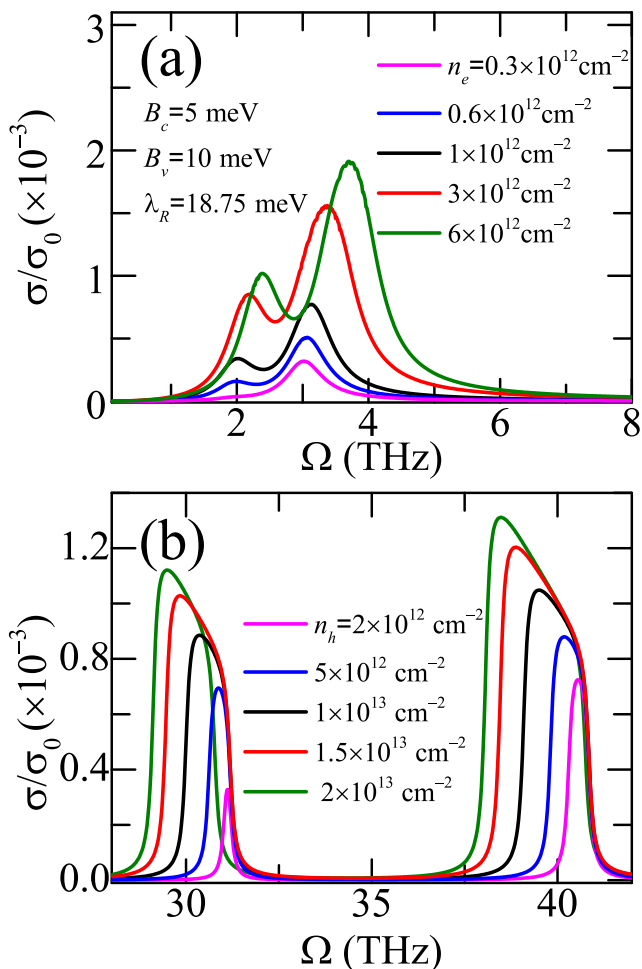


FIG. 5. Optical conductivity $\sigma(\Omega)$ as a function of radiation frequency Ω at fixed Rashba parameters $\lambda_R = 18.75$ meV, EZF parameters $B_c = 5$ meV and $B_v = 10$ meV for (a) n -type ML-MoS₂ and (b) p -type ML-MoS₂ with different electron (hole) density n_e (n_h) as indicated.

ty could be also affected by impurity or electron-phonon scattering with the modification of self-energy⁴⁶.

IV. CONCLUSIONS

In this paper, we have investigated the infrared to THz optical absorption property of n - and p -types ML-MoS₂ in the presence of proximity-induced interactions such as Rashba SOC and exchange interaction. The optical conductivity is evaluated using the standard Kubo formula under RPA by including the effective electron-electron interaction. We have examined the roles of proximity-induced interactions in affecting optical absorptions occurring in different valleys for both n - and p -type ML-MoS₂. The main conclusions obtained from this study are summarized as follows.

In the presence of proximity-induced interactions, there exist two absorption peaks in n -type ML-MoS₂ and

two knife shaped absorptions in p -type ML-MoS₂ which are contributed by the inter-subband spin-flip electronic transitions at valleys K and K' with a lifted valley degeneracy. The height and position of the absorption peaks in n -type ML-MoS₂ can be effectively tuned by Rashba parameter, EFZs parameter B_c , and electron density. The width, height, and position of the knife shaped absorptions in p -type ML-MoS₂ depend strongly on the Rashba parameter, EFZs parameter B_v , and carrier density. These features in optical conductivity curves can be explained by the electronic transition channels and the modification of conduction and valence bands by the proximity induced Rashba SOC and EZFs. The obtained results suggest that ML-MoS₂ in the presence of Rashba SOC and EZFs has a wide tunable optical response in the infrared to THz radiation regimes. The optoelectronic properties of n -type and p -type ML-MoS₂ in the presence of proximity-induced interactions can be effectively tuned by the carrier density, Rashba parameter, and EZFs which makes ML-MoS₂ a promising infrared and THz material for optics and optoelectronics. The obtained theoretical findings can be helpful for the understanding of optoelectronic properties of ML-MoS₂. We hope the theoretical predictions in this paper can be verified experimentally.

ACKNOWLEDGMENTS

This work was supported by the National Natural Science foundation of China (NSFC) (Grants No. U2230122, No. U2067207, No. 12364009, and No. 12004331), Shenzhen Science and Technology Program (Grant No. KQTD20190929173954826), and by Yunnan Fundamental Research Projects (Grants No. 202301AT070120, and No. 202101AT070166). Y.M.X. was supported through the Xingdian Talent Plans for Young Talents of Yunnan Province (Grant No. XDYC-QNRC-2022-0492).

- ¹K. S. Novoselov, A. K. Geim, S. V. Morozov, D. Jiang, Y. Zhang, S. V. Dubonos, I. V. Grigorieva, and A. A. Firsov, *Science* **306**, 666 (2004).
- ²K. F. Mak, C. Lee, J. Hone, J. Shan, and T. F. Heinz, *Phys. Rev. Lett.* **105**, 136805 (2010).
- ³Q. H. Wang, K. Kalantar-Zadeh, A. Kis, J. N. Coleman, and M. S. Strano, *Nat. Nanotech.* **7**, 699 (2012).
- ⁴T. Cao, G. Wang, W. Han, H. Ye, C. Zhu, J. Shi, Q. Niu, P. H. Tan, E. Wang, B. L. Liu, and J. Feng, *Nat. Commun.* **3**, 887 (2012).
- ⁵J. R. Schaibley, H. Yu, G. Clark, P. Rivera, J. S. Ross, K. L. Seyler, W. Yao, and X. D. Xu, *Nat. Rev. Mater.* **1**, 16055 (2016).
- ⁶D. Choi, J. Jeon, T. Park, B. Ju, and K. Lee, *Discover Nano* **18**, 80 (2023).
- ⁷X. Xu, W. Yao, D. Xiao, and T. F. Heinz, *Nat. Phys.* **10**, 343 (2014).
- ⁸J. Qi, X. Li, Q. Niu, and J. Feng, *Phys. Rev. B* **92**, 121403 (2015).
- ⁹Q. Zhang, S. A. Yang, W. Mi, Y. Cheng, and U. Schwingenschlöggl, *Adv. Mater.* **28**, 959-966 (2016).
- ¹⁰N. Cortés, F. J. Peña, O. Negrete, and P. Vargas, *Phys. Rev. B* **105**, 014443 (2022).

- ¹¹X. N. Zhao, W. Xu, Y. M. Xiao, J. Liu, B. Van Duppen, and F. M. Peeters, *Phys. Rev. B* **101**, 245412 (2020).
- ¹²D. Xiao, G. B. Liu, W. Feng, X. Xu, and W. Yao, *Phys. Rev. Lett.* **108**, 196802 (2012).
- ¹³Z. Li and J. P. Carbotte, *Phys. Rev. B* **86**, 205425 (2012).
- ¹⁴P. M. Krstajić, P. Vasilopoulos, and M. Tahir, *Phys. Rev. B* **94**, 085413 (2016).
- ¹⁵Y. M. Xiao, W. Xu, B. Van Duppen, and F. M. Peeters, *Phys. Rev. B* **94**, 155432 (2016).
- ¹⁶K. F. Mak, K. L. He, J. Shan, and T. F. Heinz, *Nat. Nanotech.* **7**, 494 (2012).
- ¹⁷B. Radisavljevic and A. Kis, *Nat. Mater.* **12**, 815 (2013).
- ¹⁸A. Splendiani, L. Sun, Y. Zhang, T. Li, J. Kim, C. Y. Chim, G. Galli, and F. Wang, *Nano Lett.* **10**, 1271 (2010).
- ¹⁹A. Soumyanarayanan, N. Reyren, A. Fert, and C. Panagopoulos, *Nature (London)* **539**, 509 (2016).
- ²⁰J. Ibañez-Azpiroz, A. Eiguren, E. Ya. Sherman, and A. Bergara, *Phys. Rev. Lett.* **109**, 156401 (2012).
- ²¹J. Ibañez-Azpiroz, A. Bergara, E. Ya. Sherman, and A. Eiguren, *Phys. Rev. B* **88**, 125404 (2013).
- ²²W. Xu, *Appl. Phys. Lett.* **82**, 724 (2003).
- ²³X. F. Wang, *Phys. Rev. B* **72**, 085317 (2005).
- ²⁴D. W. Yuan, W. Xu, Z. Zeng, and F. Lu, *Phys. Rev. B* **72**, 033320 (2005).
- ²⁵C. H. Yang, W. Xu, Z. Zeng, F. Lu, and C. Zhang, *Phys. Rev. B* **74**, 075321 (2006).
- ²⁶Y. S. Ang, J. C. Cao, and C. Zhang, *Eur. Phys. J. B* **87**, 28 (2014).
- ²⁷J. F. Sun and F. Cheng, *J. Appl. Phys.* **115**, 133703 (2014).
- ²⁸D. Xiao, W. Yao, and Q. Niu, *Phys. Rev. B* **99**, 236809 (2007).
- ²⁹G. H. Chen and M. E. Raikh, *Phys. Rev. B* **59**, 5090 (1999).
- ³⁰Z. Y. Zhu, Y. C. Cheng, and U. Schwingenschlgl, *Phys. Rev. B* **84**, 153402 (2011).
- ³¹H. Z. Lu, W. Yao, D. Xiao, and S. Q. Shen, *Phys. Rev. Lett.* **110**, 016806 (2013).
- ³²A. Kormnyos, V. Zlyomi, N. D. Drummond, and G. Burkard, *Phys. Rev. X* **4**, 011034 (2014).
- ³³A. O. Slobodeniuk and D. M. Basko, *2D Mater.* **3**, 035009 (2016).
- ³⁴E. G. Mishchenko and B. I. Halperin, *Phys. Rev. B* **68**, 045317 (2003).
- ³⁵H. Ochoa and R. Roldán, *Phys. Rev. B* **87**, 245421 (2013).
- ³⁶Q. F. Yao, J. Cai, W. Y. Tong, S. J. Gong, J. Q. Wang, X. Wan, C. G. Duan, and J. H. Chu, *Phys. Rev. B* **95**, 165401 (2017).
- ³⁷X. Liang, L. J. Deng, F. Huang, T. T. Tang, C. T. Wang, Y. P. Zhu, J. Qin, Y. Zhang, B. Peng, and L. Bi, *Nanoscale* **9**, 9502 (2017).
- ³⁸Y. Song and H. Dery, *Phys. Rev. Lett.* **111**, 026601 (2013).
- ³⁹L. Stille, C. J. Tabert, and E. J. Nicol, *Phys. Rev. B* **86**, 195405 (2012).
- ⁴⁰E. J. Nicol and J. P. Carbotte, *Phys. Rev. B* **77**, 155409 (2008).
- ⁴¹A. Paul and I. Grinberg, *Phys. Rev. A* **17**, 024042 (2022).
- ⁴²P. Leroux-Hugon, *Phys. Rev. Lett.* **29**, 939 (1972).
- ⁴³S. Chuang, C. Battaglia, A. Azcatl, S. McDonnell, J. S. Kang, X. Yin, M. Tosun, R. Kapadia, H. Fang, R. M. Wallace, and A. Javey, *Nano Lett.* **14**, 1337 (2014).
- ⁴⁴N. T. Cuong, M. Otani, and S. Okada, *J. Phys.: Condens. Matter* **26**, 135001 (2014).
- ⁴⁵H. J. Krenner, E. C. Clark, T. Nakaoka, M. Bichler, C. Scheurer, G. Abstreiter, and J. J. Finley, *Phys. Rev. Lett.* **97**, 076403 (2006).
- ⁴⁶Z. Li and J. P. Carbotte, *Physica B* **421**, 97 (2013).